

- the PTP1B-tetrapeptide complex is 0.26 Å, and those between the PTP1B-pTyr complex and the PTP1B-hexapeptide and PTP1B-tetrapeptide complexes are 0.38 and 0.40 Å, respectively. Equivalent atoms of the hexapeptide and tetrapeptide superimpose within an rms deviation of 0.54 Å. The side chain of free pTyr superimposes exactly with the side chain of pTyr within the peptides. The rotamer conformation of free pTyr differs from that of a pTyr residue in a peptide because the C α -C β bond is rotated 120° to avoid close contact of its COOH group with the side chain of Asp⁴⁸. Excluding residues 179 to 187, the rms deviation of main-chain atoms between the PTP1B-hexapeptide complex and unliganded PTP1B is 0.45 Å. The structures of unliganded wild-type and C215S PTP1B are essentially identical (Z. Jia and D. Barford, unpublished data).
25. Z.-Y. Zhang, Y. Wang, J. E. Dixon, *Proc. Natl. Acad. Sci. U.S.A.* **91**, 1624 (1994).
 26. N. Taddei *et al.*, *FEBS Lett.* **350**, 328 (1994).
 27. Z. Zhang, E. Harms, R. L. Van Etten, *J. Biol. Chem.* **269**, 25947 (1994).
 28. D. E. Knighton *et al.*, *Science* **253**, 414 (1991); E. A. Madhusudan *et al.*, *Protein Sci.* **3**, 176 (1994).
 29. R. B. Pearson and B. E. Kemp, *Methods Enzymol.* **200**, 62 (1991).
 30. Z. Songyang *et al.*, *Nature* **373**, 536 (1995).
 31. C. J. Pallen, D. S. Y. Lai, H. P. Chia, I. Boulet, P. H. Tong, *Biochem. J.* **276**, 315 (1991).
 32. The solvent-accessible surface was calculated with the program DSSP [W. Kabsch and C. Sander, *Bio polymers* **22**, 2577 (1983)].
 33. Collaborative Computational Project, Number 4, *Acta Crystallogr.* **D50**, 760 (1994).
 34. Z. Otwinowski, in *Data Collection and Processing*, L. Sawyer, N. Issacs, S. Bailey, Eds. (SERC Daresbury Laboratory, Warrington, UK, 1993), p. 56.
 35. F. C. Bernstein *et al.*, *J. Mol. Biol.* **112**, 535 (1977).
 36. A. T. Brünger, *X-PLOR, Version 3.1* (Yale Univ. Press, New Haven, CT, 1993).
 37. T. A. Jones, J. Y. Zhou, S. W. Cowan, M. Kjeldgaard, *Acta Crystallogr.* **A47**, 110 (1991).
 38. J. Navaza, *ibid.* **A50**, 157 (1994).
 39. S. V. Evans, *J. Mol. Graphics* **11**, 134 (1993).
 40. A. Nicholls, R. Bharadwaj, B. Honig, *Biophys. J.* **64**, 166 (1991).
 41. Supported by Wellcome Trust grant 042552/Z/94/Z (D.B.), Natural Sciences and Engineering Research Council of Canada (Z.J.), NIH grant CA53840 (N.K.T.), a Pew Scholar Award in the Biomedical Sciences (N.K.T.), and a Cancer Research Institute and F. M. Kirby Foundation fellowship (A.J.F.). We thank the staff at the Synchrotron Radiation Source, Daresbury, U.K.; R. M. Sweet at the National Synchrotron Light Source at Brookhaven National Laboratory, Upton, NY, for assistance with data collection; and L. N. Johnson for support and comments on the manuscript. The atomic coordinates have been submitted to the Brookhaven protein database.

6 February 1995; accepted 19 April 1995

Crystal Structure of *Pseudomonas mevalonii* HMG-CoA Reductase at 3.0 Angstrom Resolution

C. Martin Lawrence,* Victor W. Rodwell, Cynthia V. Stauffacher†

The rate-limiting step in cholesterol biosynthesis in mammals is catalyzed by 3-hydroxy-3-methylglutaryl-coenzyme A (HMG-CoA) reductase, a four-electron oxidoreductase that converts HMG-CoA to mevalonate. The crystal structure of HMG-CoA reductase from *Pseudomonas mevalonii* was determined at 3.0 angstrom resolution by multiple isomorphous replacement. The structure reveals a tightly bound dimer that brings together at the subunit interface the conserved residues implicated in substrate binding and catalysis. These dimers are packed about a threefold crystallographic axis, forming a hexamer with 23 point group symmetry. Difference Fourier studies reveal the binding sites for the substrates HMG-CoA and reduced or oxidized nicotinamide adenine dinucleotide [NAD(H)] and demonstrate that the active sites are at the dimer interfaces. The HMG-CoA is bound by a domain with an unusual fold, consisting of a central α helix surrounded by a triangular set of walls of β sheets and α helices. The NAD(H) is bound by a domain characterized by an antiparallel β structure that defines a class of dinucleotide-binding domains.

The biosynthesis of cholesterol is regulated at the level of the enzyme HMG-CoA reductase, which catalyzes the interconversion of HMG-CoA and mevalonate. This reaction is the first committed step in the pathway of isoprenoid biosynthesis. In mammals, >90% of the bulk carbon flow along this pathway is used in the production of cholesterol. Although cholesterol is an essential

component of mammalian cell membranes, its deposition in atherosclerotic plaques restricts blood flow, an important factor in heart disease and death by stroke or heart attack. The abundance of mammalian HMG-CoA reductase is normally controlled through the regulation of transcription (1), translation (2), and enzyme degradation (3), whereas the activity of the enzyme is inhibited by phosphorylation (4). Inhibition of HMG-CoA reductase by drugs such as lovastatin lowers intracellular cholesterol concentrations (5) and increases both low density lipoprotein (LDL) receptor number and absorption of cholesterol circulating as LDL (6).

The reaction catalyzed by eukaryotic HMG-CoA reductase is a four-electron

NADP(H)-dependent oxidoreduction that requires two molecules of NADPH to reduce HMG-CoA to mevalonate and CoA. The reaction is analogous to the two successive reactions of an aldehyde dehydrogenase and an alcohol dehydrogenase, but is accomplished by a single enzyme. Comparatively little is known of the structural requirements for catalysis by HMG-CoA reductase. Direct participation of cysteines in catalysis, suggested by sensitivity to sulfhydryl reagents (7–10), was disproved by elimination of cysteines by site-directed mutagenesis (11). Glutamate and histidine residues essential for catalysis have, however, been identified (11–13). Sequence analysis of >20 HMG-CoA reductases from yeast to mammals indicates a COOH-terminal catalytic domain of ~50 kD and a hydrophobic NH₂-terminal membrane-attachment domain of variable length (14). Mammalian HMG-CoA reductase is thought to be active as a homodimer with a monomer molecular size of 100 kD (15).

We have now determined the crystal structure of *Pseudomonas mevalonii* HMG-CoA reductase, a soluble protein of 45-kD subunits. Although functionally analogous to the catalytic domain of the larger mammalian enzymes, the *Pseudomonas* enzyme lacks an NH₂-terminal membrane anchor (7, 16). *Pseudomonas* HMG-CoA reductase, which functions as a catabolic enzyme, is induced by mevalonate, which it converts into HMG-CoA with NAD⁺ as an oxidant (7, 9, 17, 18). Sequence identity between the *Pseudomonas* enzyme and the COOH-terminal catalytic domain of mammalian HMG-CoA reductase is limited (20%), but key residues implicated in substrate recognition and catalysis are conserved (12, 13).

Recombinant *P. mevalonii* HMG-CoA reductase was overexpressed in *Escherichia coli* and purified to homogeneity as previously described (16). Crystals were grown in the cubic space group *I*₄32 with *a* = 229.4 Å and two monomers per asymmetric unit (19). The structure solution (Table 1) was based on an initial multiple isomorphous replacement (MIR) map calculated from four heavy-atom derivatives. The MIR phases were refined with solvent flattening and averaging over the twofold noncrystallographic symmetry, beginning at 5.0 Å and gradually extending to 3.0 Å. The final phase-refined 3.0 Å map showed continuous main chain density from the NH₂-terminus to residue 378; the last 50 residues of the molecule are disordered in the crystal. The sequence fit to the map was confirmed from the positions of the unique 24 methionines seen in difference Fourier density based on selenomethionine-substituted HMG-CoA reductase (Fig. 1). The current model has been refined with TNT (20) at 3.0 Å to give a crystallographic *R* factor of 18.9% and an

C. M. Lawrence and C. V. Stauffacher, Department of Biological Sciences, Purdue University, West Lafayette, IN 47907, USA.

V. W. Rodwell, Department of Biochemistry, Purdue University, West Lafayette, IN 47907, USA.

*Present address: Howard Hughes Medical Institute and Laboratory of Molecular Medicine, Childrens Hospital, Boston, MA 02115, USA.

†To whom correspondence should be addressed.

average *B* factor of 22.8 Å² (Table 1). Structural evaluation with the program PROCHECK (21) indicates that this refined structure has geometric parameters equal to or better than average, compared with well-refined structures at comparable resolution. All backbone (ϕ, ψ) dihedral angles fall in allowed regions in a Ramachandran plot. We have initiated structure determinations of *P. mevalonii* HMG-CoA reductase in complex with its substrates. Two separate difference Fourier studies of binary complexes have revealed the binding sites of HMG-CoA and NAD(H). Preliminary results of these studies are presented here as they both aid in interpretation of the structure and define the functional units of this enzyme.

The *P. mevalonii* HMG-CoA reductase monomer, an extended structure with overall dimensions of 70 Å by 60 Å by 30 Å, is clearly divided into a large domain and a small domain that are connected by two

nearly continuous β strands (β C- β D and β G- β H) that span the full length of the molecule (Fig. 2, A and B). The first 100 residues define two substructures: a 60-residue NH₂-terminal extension (α A through half of β A) and one face of the large domain (40 additional residues through α D). Nine residues of β chain (β C) then lay down one strand of the spanning β structure that extends into the small domain. The next 115 residues (β D through β G) form the small domain, whose fold is stabilized independently of the large domain. The following 163 residues complete the three walls of the large domain. The final COOH-terminal 50 residues, which extend from the end of α M, are not visible in the electron density.

The large domain of the HMG-CoA reductase structure has a fold not previously observed. The main body of the large domain is constructed in an unusual way, with

its major feature a 24-residue α helix (α M) that runs through the center of the domain (Fig. 2D). This helix is surrounded by three triangular walls of structure: one of a four-stranded antiparallel β sheet with a capping α helix, one of entirely α -helical structure, and a third of mixed α - β structure. The α - β wall (α D, β A, β B, α K, and α L) contains residues from both the NH₂- and COOH-terminal regions of the molecule. The wall containing the four-stranded antiparallel β structure (β C, β H, β I, β J, and α H) acts as a backbone sheet that orients the two domains through a pair of antiparallel β strands that span the molecule. The α -helical wall, a pair of antiparallel α helices (α I and α J), forms one-half of a four-helix bundle that is the major interface between monomers. The NH₂-terminal 60 residues of this domain are folded loosely into an extended arm, which appears to be nearly independent of the remainder of the large

Table 1. Data collection and structure determination. Crystals of HMG-CoA reductase were grown in the cubic space group *I*4₃₂ with *a* = 229.4 Å and two monomers per asymmetric unit, corresponding to a solvent content of 55% (19). Native and derivative data sets were collected to 2.8 Å at 4°C on a Rigaku 5-kW rotating anode equipped with two San Diego Multiwire Systems area detectors and integrated with software provided by the manufacturer (25). For the native data set, the unweighted *R*_{sym} on intensity is 5.6% (all data to 2.8 Å, 178,990 observations of 25,001 unique reflections). The heavy-atom data sets are of similar quality and exhibit changes in unit-cell parameters of <0.2%. The fluorescein mercuric acetate (FMA) difference Patterson map was interpreted with a graphical method to determine the positions of FMA in the crystal. Heavy-atom positions in subsequent derivatives were identified in difference Fourier maps. Refinement of heavy-atom parameters and calculation of MIR phases to 3.0 Å were performed with the program HALSQ (M. G. Rossmann), giving an overall figure of merit of 0.65. All derivatives share one common site located on the noncrystallographic twofold axis; the FMA and KAuCl₄ (1 and 2) derivatives share two sites, whereas the two KAuCl₄ derivatives have three sites in common. The inclusion of these common sites artificially inflates the MIR figure of merit. Rotation functions and heavy-atom positions each failed to define a unique molecular twofold axis; thus, initial phase improvement through density modification was limited to solvent flattening with the Wang-Leslie procedure implemented in the CCP4 program suite (26). An initial mask was generated at 5 Å with a conservative 30% solvent content, and was increased stepwise to 48% solvent. The solvent flattening was then extended in steps of one reciprocal lattice point from 5.0 to 3.0 Å resolution. The MIR, solvent-

flattened map showed 16 well-defined globular densities of 130 Å diameter in the unit cell, each centered around a threefold crystallographic axis. At this point, recognizable secondary structure elements defined the position of a molecular twofold symmetry axis. The inability of the heavy-atom positions to define the axis was explained by their asymmetrical location in only one-half of the molecule or on the noncrystallographic twofold axis. The positions of the molecular twofold axes were perpendicular to the crystallographic threefold axes, defining a packing arrangement with 23 symmetry. This arrangement was confirmed in a general self-rotation function with the program GRLF (27). The position of the molecular twofold axis was then refined in real space and the map was averaged about this axis with programs from the AVGSYS package (28). An initial polyalanine tracing of the structure was built into the once averaged map with the program FRODO (29). With a mask generated from the smeared polyalanine coordinates, cycles of combined molecular averaging and solvent flattening were begun at 5.0 Å resolution and extended to 3.0 Å in steps of a single reciprocal lattice point with a combination of CCP4 and AVGSYS programs. A full model of the HMG-CoA reductase structure was built into the final 3.0 Å averaged, solvent-flattened map with the fragment search option of the program O (30). The sequence fit to the map was confirmed with data from selenomethionine-substituted HMG-CoA reductase (Fig. 1). The model was improved in cycles of crystallographic refinement with TNT (20) interleaved with manual rebuilding. The current model has been refined at 3.0 Å resolution to give a crystallographic *R* factor of 18.9% and an average *B* factor of 22.8 Å². The root mean square deviations from ideal bond distances and angles are 0.019 Å and 2.02°, respectively.

Data set	Resolution (Å)	Unique reflections	Redundancy*	Completeness† (%)	<i>R</i> _{sym} ‡ (%)	<i>R</i> _{scale} § (%)	Refined sites	Phasing power
Native	2.8	25,001	7.2	100	5.6			
FMA	2.8	22,908	5.2	83.8	7.4	14.1	2	2.16
KAuCl ₄ (1)	3.0	13,717	4.9	70.3	6.6	14.2	4	1.78
KAuCl ₄ (2)	3.0	19,955	6.1	100	6.0	13.7	5	1.51
KAu(CN) ₂	3.0	17,820	5.8	91.3	6.4	12.3	1	1.99

Parameter	Figure of merit distributions									
Resolution (Å)	10.00	6.67	5.00	4.00	3.33	2.86	Total			
Overall FOM¶	0.704	0.733	0.750	0.720	0.648	0.559	0.650			
Number per zone	500	1,404	2,644	4,268	6,233	7,554	22,603			
Figure of merit	0.05	0.15	0.25	0.35	0.45	0.55	0.65	0.75	0.85	0.95
Number per bin	605	895	1,312	1,543	1,942	2,227	2,640	3,279	4,052	4,108

*Redundancy, total number of observed reflections divided by the number of unique reflections. †Completeness to indicated resolution. ‡*R*_{sym} = $\sum_n |I_n - \langle I_n \rangle| / \sum_n \langle I_n \rangle$, where *I_n* is the average intensity of reflection *n* and *I_n* is the individual measured intensity for each occurrence *i* of the reflection *n*. §*R*_{scale} = $\sum_n |F_{PH} - F_N| / \sum |F_N|$, where *F_{PH}* and *F_N* are the measured structure factors from the heavy-atom derivative and the native crystals, respectively. ||Phasing power is calculated as the ratio *f_H*/*ε*, where *f_H* is the heavy-atom structure factor and *ε* is the root mean square lack of closure error. ¶FOM, figure of merit for reflections within the designated resolution zone.

domain. An antiparallel pair of helices (αA , αB) folds on the exterior of the molecule, followed by an extended loop carrying helix αC . A long β strand (βA) runs from this loop back to the compact portion of the domain, twisting through 180° as it crosses the molecule and enters the triangular structure as one of the β strands of the α - β wall. The loop between helix αC and βA in this portion of the structure contains one of the highly conserved sequences of HMG-CoA reductase, EX_3GX_4P (Table 2).

Although *P. mevalonii* HMG-CoA reductase uses NAD(H) as a cofactor, it lacks any structure comparable to the classic dinucleotide-binding fold, a six-stranded parallel β sheet with right-handed crossover helices connecting the NH_2 - and $COOH$ -termini of the sheet strands (22). The small domain of HMG-CoA reductase defines another class of dinucleotide-binding fold composed of a four-stranded antiparallel β sheet with two crossover helices that lie across one side of the sheet (Fig. 2C). The first turns of the second crossover helix (αG) and the preceding loop contain the sequence DAMGXN, another signature sequence for HMG-CoA reductase (Table 2).

The packing of the subunits in the crystal reveals a dimer with an extensive inter-

subunit interface formed by the two monomers in the asymmetric unit (Fig. 3). A solvent-inaccessible surface area of 4800 \AA^2 per monomer, 28% of the total monomer surface, is buried at the dimer interface. The center of the dimeric structure contains a familiar motif, an antiparallel four-helix bundle. Each monomer contributes two helices (αI and αJ), which cross the corresponding pair at a standard helix interaction angle. In contrast to a typical hydrophobic core, the core of this motif is rich in salt bridges between acidic and basic residues. The intersubunit contacts between the large and small domains form another important interaction in the dimer. The β strands of the small domain, which in the monomer extend like the fingers of an open hand, wrap around helix αH in the large domain of the twofold-related monomer.

The NH_2 -termini of the two subunits, which appear loosely folded in the monomer, form the most complex of the intersubunit interactions (Fig. 3). The NH_2 -terminal arm of the large domain reaches toward the large domain of the symmetry-related monomer, placing the EX_3GX_4P loop of one monomer adjacent to the catalytic E83 loop (Table 2) of the opposite monomer. The βA strands from each

monomer then cross back toward their own subunits, running antiparallel to each other for 11 residues in a twisted β ribbon. A reverse turn aligns strand βB antiparallel to βA , creating a small three-strand sheet in each domain connected across the twofold axis by the βA ribbon structure. These interactions loop the NH_2 -terminal arm of one monomer around the NH_2 -terminal arm of the opposite monomer. This unusual structure is fully dependent on dimer formation, implying that the first 50 to 60 residues of the subunit must remain partially structured during early assembly of the active enzyme.

The monomer interactions of the HMG-CoA reductase subunits described above result in a T-shaped dimer (Fig. 3) with dimensions of 70 \AA by 60 \AA by 50 \AA . The dimer axis runs vertically through the stem of the T, whereas the dimer interface lies roughly in the plane of the figure. The small domains and the backbone β sheets cross the T, and the four-helix bundle is located at the center of the stem. Two large open cavities of approximate dimensions 15 \AA by 15 \AA by 20 \AA are formed at the intersection of the stem with the top of the T-shaped dimer. The NH_2 -termini are located at the foot of the T-shaped mole-

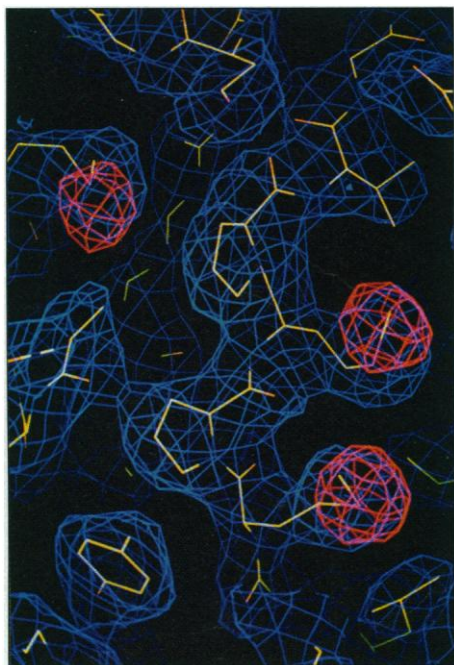


Fig. 1. Selenomethionine difference Fourier density (magenta), superimposed on the $2F_o - F_c$ map (blue) (F_o , observed structure factor; F_c , calculated structure factor), in the region of the backbone sheet of the large domain of HMG-CoA reductase. A Met-Pro-Met-Pro sequence of the central strand runs from bottom to top. Clear spherical density appears at the positions of the 24 methionines in the asymmetric unit of the crystal superimposed on the S atom of methionines of the initial sequence fit.

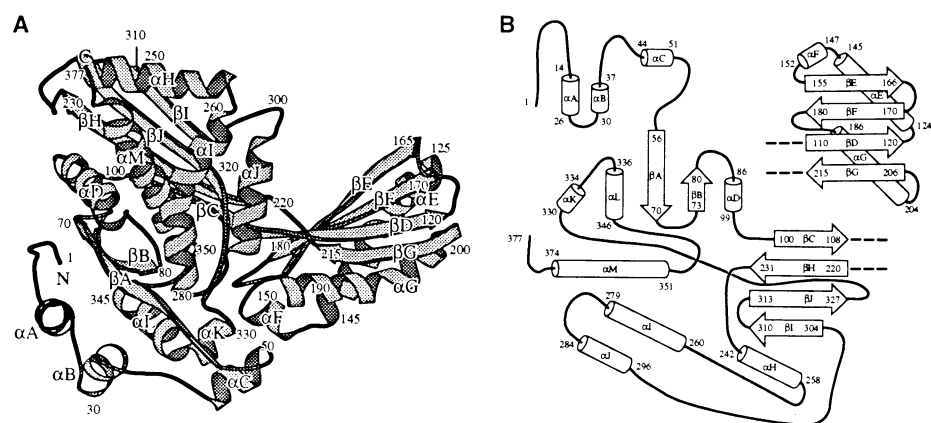


Fig. 2. Structure and topology of *P. mevalonii* HMG-CoA reductase. Ribbon drawings were generated by the program MOLSCRIPT (31). **(A)** Ribbon drawing of the HMG-CoA reductase monomer generated from the 3.0 \AA TNT-refined coordinates. The molecule is oriented with the large domain on the left, the small domain on the right, and the extended NH_2 -terminal tail on the lower left. N and C, NH_2 - and $COOH$ -termini, respectively. **(B)** "Exploded" α helix- β strand representation of the topology of the large domain (left) and small domain (right). Structural elements and residue numbers are shown in both (A) and (B). **(C)** The small domain of the molecule viewed roughly parallel to the β sheet with αE and αF positioned at the back of the view. The conserved DAMGXN sequence extending into αG is highlighted in black. **(D)** The large domain of the molecule viewed approximately parallel to the long axis of the central α helix. The α - β wall is to the left, the all- α wall to the right, and the β sheet wall with capping α helix at the top of this triangular structure. The extended NH_2 -terminal arm (bottom) contains the EX_3GX_4P loop (highlighted in black). The highlighted loop near the center of this domain contains the catalytic E83 loop. A, Ala; D, Asp; E, Glu; G, Gly; M, Met; N, Asn; P, Pro; X, unspecified amino acid.

cule. Although *P. mevalonii* HMG-CoA reductase lacks the flexible linker and the NH₂-terminal membrane-anchor domains of eukaryotic HMG-CoA reductases, the position of the NH₂-termini suggests that the membrane domains in the eukaryotic enzymes would emanate from the foot of a similar T-shaped dimer of catalytic subunits.

Difference Fourier studies have revealed the binding sites in the binary enzyme-

substrate complexes for HMG-CoA and NAD(H). These studies show that the two open cavities formed at the dimer interface contain the two active sites of the molecule (Fig. 3). HMG-CoA is bound predominantly by the large domain of one monomer and NAD(H) by the small domain of the symmetry-related monomer (Fig. 4). These binding sites bring the two substrates together at the dimer interface, such that the thioester of HMG-CoA and C-4 of the

nicotinamide ring of NAD(H) are within 3.5 Å of one another in the active site. Dimerization is thus a prerequisite for formation of an active site in this enzyme.

Regions of conserved sequence in the family of HMG-CoA reductases (Table 2) are located in or around the active site cavity. Two conserved NH₂-terminal regions, one from each monomer, contribute to the formation of one rim of the active site (Fig. 4). The βB-αD loop (Fig. 4, blue monomer) lies along one edge of the cavity with the side chain of its Glu⁸³ residue pointing straight down into the active site. This loop is constrained by hydrogen bonds between the side chain of Glu⁵² of the EX₃GX₄P loop (red monomer) and main chain amides of the E83 loop (blue monomer). An intersubunit salt bridge between Glu⁸² and Arg²⁸⁵ also constrains the configuration of the active site E83 loop.

A third conserved region near the active site is the DAMGXN sequence, which is located in the small domain (Fig. 4, red monomer). The loop and NH₂-terminal portion of the helix that constitute this conserved region point down into the active site from the rim of the cavity opposite to the E83 loop. The GX₂G₂XT motif present in the loop and first turn of helix αK in the large domain is also found along the rim of the active site, where it lies adjacent to the DAMGXN motif of the small domain (Fig. 4, blue monomer). A fifth conserved region (Table 2), located immediately beyond the end of the defined structure, contains His³⁸¹, a residue that is important in catalysis (12). This region begins at the end of the long central helix (αM) (Fig. 4, blue monomer) immediately adjacent to the active site. Additional conserved residues located in the active site include Lys²⁶⁷, Asn²⁷¹, and Asp²⁸³.

HMG-CoA is bound by the large domain (Fig. 4, blue monomer) in an extended form that stretches across the active site cavity. The adenine and ribose phosphate moieties lie in a pocket formed by the NH₂-terminal residues (6 through 13) and helix αD. The EX₃GX₄P loop in the arm of the large domain of the symmetry-related monomer closes around the adenine at one end of the pocket, whereas βA runs underneath these groups, forming the pocket floor. Shifts in the positions of basic residues in the vicinity of the ribose phosphate indicate binding interactions. The diphosphopantetheine moiety extends across Ala⁸⁸ of helix αD and into the active site. In this rough fit, the scissile bond of the thioester of HMG-CoA is within reach of the glutamyl side chain of Glu⁸³.

The NAD(H) molecule is bound primarily to the small domain of HMG-CoA

Table 2. Signature sequences of HMG-CoA reductase. Listed are regions that have been assigned specific functions in catalysis (12) or ligand binding (indicated by the green structures in Figs. 3 and 4).

Designation*	Residues	Location	Proposed function
EX ₃ GX ₄ P	52 to 61	αC-βA loop and strand	HMG-CoA binding
E83 loop	81 to 88	βB-αD loop and helix	Catalysis, HMG-CoA binding
DAMGXN	183 to 188	βF-αG loop and helix	NAD(H) binding
GX ₂ G ₂ XT	326 to 332	βI-αK loop and helix	NAD(H) binding
H381	377 to 428	Undefined (flexible domain)	Catalysis

*E, Glu; G, Gly; P, Pro; D, Asp; A, Ala; M, Met; N, Asn; T, Thr; H, His; and X, unspecified amino acid.

Fig. 3. The T-shaped HMG-CoA reductase dimer viewed perpendicular to the molecular twofold (vertical axis). The two monomers are colored in red and blue. The intersubunit interactions of the small domains and the NH₂-terminal arms are shown at the top and bottom, respectively. The central four-helix bundle is buried in the center of the molecule and is obscured by the strands of the backbone sheet of the blue monomer. The small subunits curl around the αH helix in the arms of the T, to the left and right. The twisted β ribbon-β sheet structure formed by the NH₂-termini is at the bottom, where the crossover of the αC loop and βA strands is apparent. The membrane-anchoring domain of the eukaryotic enzymes would presumably extend down into the membrane from the bottom of the dimer. Arrows, positions of the active sites at the junction of the top and stem of the T; green regions, conserved signature sequences of HMG-CoA reductases that line the edges of the active site pockets.



Fig. 4. The active site of *P. mevalonii* HMG-CoA reductase, viewed in stereo, looking directly into one of the dimer interface active site cavities. This view corresponds to a 90° rotation about the twofold axis of the view shown in Fig. 3. The conserved sequences that line the rim of one of the two active sites in the molecule are highlighted in green. Structural elements for the EX₃GX₄P and DAMGXN sequences are contributed by the red subunit. The catalytic E83 loop and the GX₂G₂XT sequence are contributed by the blue subunit. The catalytic H381 conserved sequence, which is in the proposed flap domain extending from the long helix (αM), is contributed by the blue subunit (arrow). Positions of the HMG-CoA and NAD(H) molecules were determined from difference Fourier maps of the individual binary complexes. HMG-CoA (orange) is shown on the left, bound to the blue subunit; NAD(H) (yellow) is on the right, bound to the red subunit.

reductase. The β F- α G loop runs under the adenine ring and then into helix α G, whereas helix α F runs over the adenine to sandwich the ring between the DAM residues of the DAMGXN motif and helix α F. The 2'- and 3'-OH groups of the adenine ribose are hydrogen-bonded by Asp¹⁴⁶ and Thr¹⁸⁹, respectively, whereas the NH₂-terminus of helix α G, GXN of the DAMGXN motif, interacts with the diphosphate moiety of the NAD(H) through the unsaturated amide nitrogens of the helix and the asparagine side chain. Although this subunit has an unusual type of dinucleotide-binding fold, the interactions of the diphosphate of NAD(H) with the NH₂-terminus of helix α G are similar to those in the classic dinucleotide-binding fold. The large domain also participates in binding the NAD(H) cofactor. The main chain amides of the GX₂G₂XT loop interact with the diphosphate moiety, whereas Asn²¹⁶ and Asp²⁸³ are in position to interact with the carboxamide group of the nicotinamide ring. Binding of NAD(H) in this manner positions the nicotinamide ring adjacent to the scissile bond of HMG-CoA.

The results of the two difference Fourier studies show that when either HMG-CoA or NAD(H) is bound to the enzyme in the absence of the other, the active site is exposed to the solvent. Typically, hydride ion transfer occurs in an active site that excludes solvent. A solvent-exposed active site also seems unlikely because release of the putative aldehyde intermediate formed between the first and second steps in the reaction has not been detected. In addition, the COOH-terminal 50 residues of the *P. mevalonii* HMG-CoA reductase molecule, which are disordered in the structure, contain a highly conserved histidine residue, His³⁸¹, that is essential for catalysis (12, 13). This residue is only five amino acids beyond the end of the ordered density at the COOH-terminus of α M, the central helix of the large domain. Given these considerations, we propose that the COOH-terminal 50 residues form a third domain, a movable flap that closes over the active site when all substrates are in place. This enclosure would both position the catalytic residue His³⁸¹ in the active site and isolate the reaction from the solvent.

Structure-based parallels suggest an explanation for a control mechanism for this enzyme in mammals. The activity of HMG-CoA reductase in higher eukaryotes is controlled by the phosphorylation of a single serine residue, which in the mammalian enzyme is located six residues beyond the catalytic histidine (4, 23). From sequence comparisons, this serine residue would also be located on the proposed flexible portion

of the structure, which, although containing fewer residues than in the *P. mevalonii* enzyme, could also close over the active site on substrate binding. When phosphorylated, the corresponding serine of hamster HMG-CoA reductase appears to interact with the catalytic histidine (24). This interaction could interfere with closure of the COOH-terminal flexible domain, and thereby control enzyme activity.

Although previous studies of the multimeric state of *P. mevalonii* HMG-CoA reductase suggested the enzyme was a homotetramer (17), the crystal structure reveals a dimer with an extensive subunit interface. However, in the crystal, the dimers are themselves in contact with each other about a crystallographic threefold axis. This trimeric arrangement of dimers results in a hexamer with 23 symmetry (D₃ symmetry). Within the hexameric arrangement, the intersubunit interactions between dimers include contacts between the NH₂-terminal half of helix α E of a small domain and the backbone β sheet of the large domain of an adjacent dimer. In addition to the 4800 Å² of solvent-inaccessible surface created in formation of the dimer, an area of 1100 Å² is buried in each of the six repeated interactions that participate in formation of the hexamer. These observations suggest that the *P. mevalonii* enzyme may in fact exist in vivo as a hexamer, or as an equilibrium mixture of dimers and hexamers.

The solution of the first structure of an HMG-CoA reductase has important implications for understanding cholesterol biosynthesis and its control in humans. These studies provide the opportunity to build the structure of mammalian HMG-CoA reductase on that of the *P. mevalonii* enzyme, to model the binding of anticholesterol drugs, to identify elements of the active site that interact with these inhibitors, and to apply the results further to model enzyme-drug interactions.

REFERENCES AND NOTES

1. T. F. Osborne, J. L. Goldstein, M. S. Brown, *Cell* **42**, 203 (1985); C. F. Clarke, A. M. Fogelman, P. A. Edwards, *J. Biol. Chem.* **260**, 14363 (1985); T. F. Osborne, G. Gill, J. L. Goldstein, M. S. Brown, *ibid.* **263**, 3380 (1988).
2. J. L. Goldstein and M. S. Brown, *Nature* **343**, 425 (1990).
3. D. J. Chin *et al.*, *Mol. Cell. Biol.* **5**, 634 (1985); D. G. Scalinick, H. Narita, C. Kent, R. D. Simoni, *J. Biol. Chem.* **263**, 6836 (1988); K. T. Chun and R. D. Simoni, *ibid.* **267**, 4236 (1992); J. Roitelman, E. H. Olender, S. Bar-Nun, W. A. Dunn Jr., R. D. Simoni, *J. Cell Biol.* **117**, 959 (1992).
4. P. R. Clarke and D. G. Hardie, *EMBO J.* **9**, 2439 (1990); G. Gillespie and D. G. Hardie, *FEBS Lett.* **306**, 59 (1992).
5. P. Louis-Flamberg *et al.*, *Biochemistry* **29**, 4115 (1990); A. Endo, *J. Lipid Res.* **33**, 1569 (1992).
6. M. S. Brown and J. L. Goldstein, *Science* **232**, 32 (1986).
7. T. C. Jordan-Starck and V. W. Rodwell, *J. Biol. Chem.* **264**, 17913 (1989).
8. M. E. Kirtley and H. Rudney, *Biochemistry* **6**, 230 (1967); J. Roitelman and I. Shechter, *J. Lipid Res.* **30**, 97 (1989).
9. J. F. Gill Jr., M. J. Beach, V. W. Rodwell, *J. Biol. Chem.* **260**, 9393 (1985).
10. R. E. Dugan and S. S. Katiyar, *Biochem. Biophys. Res. Commun.* **141**, 278 (1986).
11. T. C. Jordan-Starck and V. W. Rodwell, *J. Biol. Chem.* **264**, 17919 (1989).
12. Y. Wang, B. G. Darnay, V. W. Rodwell, *ibid.* **265**, 21634 (1990); B. G. Darnay, Y. Wang, V. W. Rodwell, *ibid.* **267**, 15064 (1992).
13. B. G. Darnay and V. W. Rodwell, *ibid.* **268**, 8429 (1993).
14. E. H. Olender and R. D. Simoni, *ibid.* **267**, 4223 (1992).
15. P. A. Edwards, E. S. Kempner, S.-F. Lan, S. K. Erickson, *ibid.* **260**, 10278 (1985); R. J. Mayer, C. Debouck, B. W. Metcalf, *Arch. Biochem. Biophys.* **267**, 110 (1988).
16. M. J. Beach and V. W. Rodwell, *J. Bacteriol.* **171**, 2994 (1989).
17. J. F. Gill Jr., M. J. Beach, V. W. Rodwell, *ibid.* **160**, 294 (1984).
18. Y. Wang, M. J. Beach, V. W. Rodwell, *ibid.* **171**, 5567 (1989).
19. C. M. Lawrence, Y.-I. Chi, V. M. Rodwell, C. V. Stauffer, *Acta Crystallogr.* **D51**, 386 (1995).
20. D. E. Tronrud, L. F. Ten Eyck, B. W. Matthews, *ibid.* **A43**, 489 (1987).
21. R. A. Laskowski, M. W. MacArthur, D. S. Moss, J. M. Thornton, *J. Appl. Crystallogr.* **26**, 283 (1993).
22. G. E. Schulz, *Curr. Opin. Struct. Biol.* **2**, 61 (1992).
23. P. R. Clarke and D. G. Hardie, *FEBS Lett.* **269**, 213 (1990).
24. R. V. Omkumar and V. W. Rodwell, *J. Biol. Chem.* **269**, 16862 (1994).
25. N.-H. Xuong, D. Sullivan, C. Nielsen, R. C. Hamlin, D. H. Anderson, *Acta Crystallogr.* **B41**, 267 (1985); N.-H. Xuong, C. Nielsen, R. C. Hamlin, D. H. Anderson, *J. Appl. Crystallogr.* **18**, 342 (1985).
26. B. C. Wang, *Methods Enzymol.* **115**, 90 (1985); A. G. W. Leslie, in *Aspects of Protein Crystal Analysis*, J. R. Helliwell, P. A. Machin, M. Z. Papiz, Eds. [Science and Engineering Research Council (SERC), Daresbury Laboratory, Daresbury, UK, 1987], pp. 35-90; CCP4, *The SERC (UK) Collaborative Computing Project No. 4, A Suite of Programs for Protein Crystallography* (Daresbury Laboratory, Warrington, UK).
27. L. Tong and M. G. Rossmann, *Acta Crystallogr.* **A46**, 783 (1990).
28. J. T. Bolin, J. L. Smith, S. W. Muchmore, in *Abstracts of the American Crystallographic Association: Series 2*, Albuquerque, NM, 22 to 28 May 1993 (American Crystallographic Association, Buffalo, NY, 1993).
29. T. A. Jones, *Methods Enzymol.* **115**, 157 (1985); *J. Appl. Crystallogr.* **11**, 268 (1978); J. W. Pflugrath, M. A. Saper, F. A. Quiocho, in *Methods and Applications in Crystallographic Computing*, S. Hall and T. Ashida, Eds. (Oxford Univ. Press, London, 1984), pp. 404-407.
30. T. A. Jones and S. Thirup, *EMBO J.* **5**, 819 (1986); T. A. Jones, J. Y. Zou, S. W. Cowan, M. Kjeldgaard, *Acta Crystallogr.* **A47**, 110 (1991).
31. P. J. Kraulis, *J. Appl. Crystallogr.* **24**, 946 (1991).
32. We thank T. Jordan-Starck, Y. Wang, B. Darnay, D. Bochar, and K. Rogers for help with the biochemical aspects of this project; the members of the Markey Center for Structural Biology group at Purdue for support in the crystallographic structure solution; J. Bolin, J. Smith, and W. Cramer for their insightful comments and editorial help; and J. Bell, S. Fateley, M. O'Neil, and A. Bunker for help in producing the manuscript. Supported by an American Heart Association predoctoral fellowship to C.M.L., NIH grant HL 47113 to V.W.R., and grant-in-aid 91014190 from the American Heart Association and support from the Markey Center for Structural Biology to C.V.S. Support for the area detectors, graphics workstations, and computational facilities was provided in part by the Center for AIDS Research, funded by NIH grant AI 127713.

23 March 1995; accepted 28 March 1995